

# Spin dynamics in the linear-chain $S=1$ antiferromagnet $\text{Ni}(\text{C}_3\text{H}_{10}\text{N}_2)_2\text{N}_3(\text{ClO}_4)$

A. Zheludev

*Department of Physics, Brookhaven National Laboratory, Upton, New York 11973-5000*

S. E. Nagler\*

*Department of Physics and the Center for Ultralow Temperature Research, University of Florida, Gainesville, Florida 32611-8440*

S. M. Shapiro

*Department of Physics, Brookhaven National Laboratory, Upton, New York 11973-5000*

L. K. Chou and D. R. Talham

*Department of Chemistry, University of Florida, Gainesville, Florida 32611-7200*

M. W. Meisel

*Department of Physics and the Center for Ultralow Temperature Research, University of Florida, Gainesville, Florida 32611-8440*

(Received 15 November 1995)

Magnetic excitations in the quasi-one-dimensional Heisenberg spin-1 antiferromagnet  $\text{Ni}(\text{C}_3\text{H}_{10}\text{N}_2)_2\text{N}_3\text{ClO}_4$  (NINAZ) have been studied by single-crystal inelastic neutron scattering. A Haldane gap  $\Delta \approx 3.6$  meV in the spin excitation spectrum was observed in the vicinity of the antiferromagnetic wave vector at low temperature and the dispersion relation was measured. The temperature dependence of the energy gap  $\Delta(T)$  was measured in the range 8–50 K and was found to be inconsistent with the predictions of the quantum nonlinear  $\sigma$  model. The results are discussed in comparison with those found in the literature for similar systems. [S0163-1829(96)02022-X]

## I. INTRODUCTION

Interest in low-dimensional quantum magnetism was strongly renewed in 1983 by the theoretical results of Haldane.<sup>1,2</sup> Applying continuum field-theoretical models one-dimensional (1D) Heisenberg quantum antiferromagnets (AF's), he suggested that for *integer* spin systems the ground state is a nonmagnetic singlet with an exchange-induced energy gap  $\Delta$  in the magnetic excitation spectrum.

Since this breakthrough, much theoretical work<sup>3–6</sup> has been aimed at clarifying the nature of the Haldane ground state and the low-lying magnetic excitations. Among the most important theoretical and numerical predictions is the fact that near the AF wave vector ( $q = \pi/a$ ,  $a$  being the interspin spacing) the magnetic excitations are well defined and spin-wave-like. It was also demonstrated that the Haldane phase is not destroyed by weak interchain interactions<sup>8,9</sup> and single-ion easy-plane anisotropies<sup>10–12</sup> found in real quasi-1D materials. The first excited state is threefold degenerate in the isotropic (Heisenberg) case. In the case of easy-plane anisotropy the excitation spectrum consists of a lower-lying doublet, with the associated  $\Delta^\perp$  (fluctuations of spin components perpendicular to  $x$ , the chain direction), and a higher-energy singlet with  $\Delta^{xx}$ .

The Haldane conjecture was first put to the test by numerical simulations.<sup>7,10,12–15</sup> Experimental support for the theory was obtained by studying several quasi-1D spin-1 antiferromagnetic materials (for a comprehensive reference list see Ref. 16). In this paper we present our single-crystal inelastic neutron scattering studies of the Haldane-gap system  $\text{Ni}(\text{C}_3\text{H}_{10}\text{N}_2)_2\text{N}_3(\text{ClO}_4)$  (NINAZ).<sup>17–19</sup> This material is

structurally related to the extensively studied  $[\text{Ni}(\text{C}_2\text{MgN}_2)_2]\text{NO}_2(\text{ClO}_4)$  (NENP) (Refs. 16,20,21) and  $[\text{Ni}(\text{C}_3\text{H}_{10}\text{N}_2)_2]\text{NO}_2(\text{ClO}_4)$  (NINO).<sup>22,23</sup> Unlike these two other compounds, where  $J$  is of the order of 50 K, the exchange constant in NINAZ is larger, approximately 145 K, as deduced from magnetic susceptibility and optical birefringence measurements.<sup>17</sup> This allows a test of the applicability of Haldane's theory within one family of structurally related materials, but on a different energy scale. The larger energy scale of NINAZ makes it easier to explore the temperature dependence of the Haldane gap and other quantities of interest in the important limit  $T \ll \Delta$ .

## II. EXPERIMENT

The crystal structure of NINAZ has been studied by Gadet *et al.*<sup>17</sup> At room temperature it is orthorhombic, with the cell constants  $a = 5.86$  Å,  $b = 8.28$  Å, and  $c = 15.15$  Å, the space group being  $Pn2n$ . The  $\text{Ni}^{2+}$  ions, each carrying spin  $S=1$ , are arranged in chains along the  $a$  axis (the  $x$  direction), the compound being strongly one dimensional. The single-ion anisotropy is expected to be of easy-plane character. Notably, in NINAZ (unlike NENP) there is only one Ni site per unit cell, and the 1D AF wave vector is  $\pi/a$ .

NINAZ single-crystal samples were grown at the University of Florida particularly for our experiments. The samples were synthesized using a method similar to that of Gadet *et al.*<sup>17</sup> Complete details of the sample preparation protocols are given elsewhere.<sup>24</sup> Well-shaped hexagonal deep blue single crystals were obtained by growth out of an aqueous solution. Preliminary neutron scattering work has been performed on a protonated sample (sample A),  $\approx 0.36$  cm<sup>3</sup> in

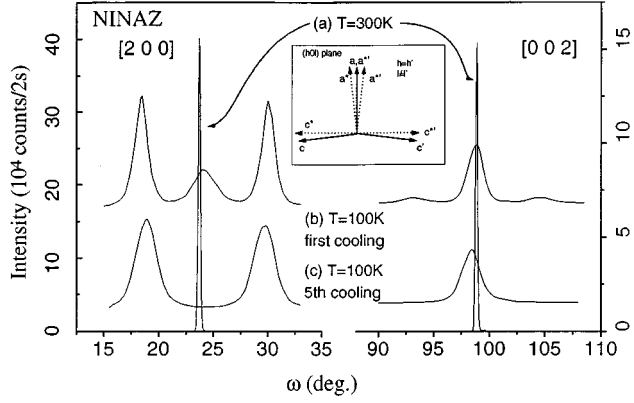


FIG. 1. Crystal mosaic of the deuterated NINAZ sample B before cooling (a), peak splitting upon first cooling (b), and after cycling the sample several times through the phase transition (c). Inset: schematic representation of the twinning in the low-temperature monoclinic phase.

volume. More accurate data were later collected using a fully deuterated sample (sample B),  $\approx 0.2 \text{ cm}^3$ .

The inelastic neutron scattering experiments were carried out on the H4M triple-axis spectrometer at the High Flux Beam Reactor at the Brookhaven National Laboratory. Most of the data were collected with a fixed final neutron energy of 14.7 meV. A pyrolytic graphite filter was positioned after the sample to reduce higher-order beam contamination. Several collimation setups were used to meet the conflicting needs of resolution and intensity. A typical  $40' - 20' - 40' - 40'$  setup provided an energy resolution of  $\delta E = 0.7 \text{ meV}$  at  $Q = [1.5 \ 0 \ 0]$ ,  $\Delta E = 0$ . The crystals were wrapped in aluminum foil, and mounted in a standard Displex refrigerator such that the (010) crystallographic planes lay in the scattering plane of the spectrometer. Thus measurements could be performed in the temperature range 7–300 K, and wave vectors of type  $[h \ 0 \ l]$  were accessible.

The experiments were complicated by the fact that at  $T \approx 260 \text{ K}$  NINAZ undergoes a structural phase transition,<sup>17</sup> accompanied by a deterioration of the crystal. The low-temperature structure is not known precisely to date. It appears to be monoclinic, with  $b$  the unique axis, and  $\beta \approx 95^\circ$ . The crystal splits, presumably on the microscopic scale, into two domains, the  $a$  (chain) and  $b$  (unique) axes being common to both domain types. The phase transition and domain formation was observed by monitoring some of the Bragg peaks while sweeping the sample temperature. The low-temperature cell constants were determined:  $a = 5.722 \text{ \AA}$ ,  $c = 15.328 \text{ \AA}$ , and  $\beta = 95.37^\circ$ . Figure 1 illustrates the effects of the phase transition on the crystal mosaic. The mosaic spread of the crystals as grown is very small [ $\approx 0.3^\circ$ , Fig. 1(a)]. After slowly cooling once to low temperatures, the mosaic increased irreversibly to a few degrees full width at half maximum (FWHM), and split into domains, most of which had a common  $a$  axis characterized by the splitting of the  $[h \ 0 \ 0]$  peaks in a rocking curve [Fig. 1(b)]. A residual part of the crystal was split into domains having a common  $c$  axis, leading to some scattering at the original  $[h \ 0 \ 0]$  positions and splitting of  $[0 \ 0 \ k]$  peaks. After thermal cycling, the sample mosaic reached a stable configuration [Fig. 1(c)], with all of the domains having a

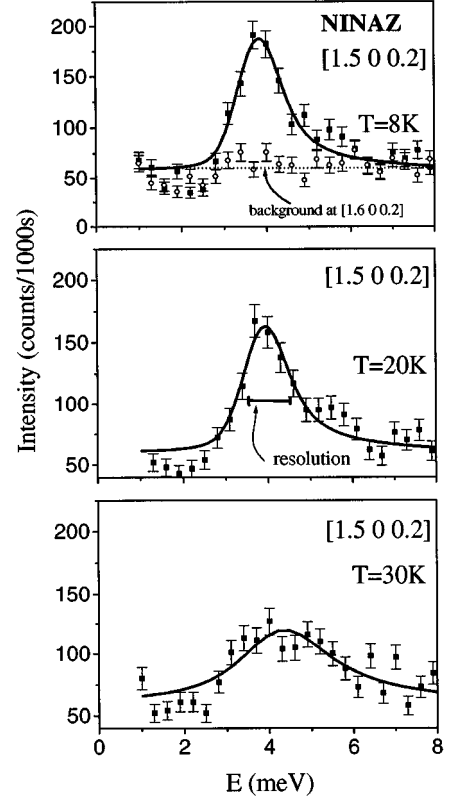


FIG. 2. Energy scans (raw data) taken at  $Q = [1.5 \ 0 \ 0.2]$  on the deuterated sample B of NINAZ at several temperatures. The solid lines represent fits described in the text. The open circles in the uppermost panel show the nonmagnetic background measured at 8 K at  $Q = [1.6 \ 0 \ 0.2]$ . The dotted line is the average constant background. The horizontal bar shows the FWHM of the energy-projected resolution function ( $\approx 0.95 \text{ meV}$  at  $\hbar\omega = 4.5 \text{ meV}$ ).

common  $a$  axis. Fortunately, for the quasi-1D case, the spin wave dispersion *perpendicular* to the chain direction is expected to be very small. This implies that the magnetic inelastic scattering depends only on the projection of the scattering vector on the  $a$  direction, and the magnetic scattering function may be approximated as  $S(\mathbf{q}, \omega) \approx S(q_{\parallel}, \omega)$ , where  $q_{\parallel} = (\mathbf{q} \cdot \mathbf{a})/a^2$ . The validity of this approximation was tested by measuring the dispersion along  $c^*$ , as described below. The two types of domains, sharing a common  $a$  axis, should therefore give equal contributions to the magnetic scattering.

### III. RESULTS AND DISCUSSION

#### A. Measurements of $S^{\perp}(\mathbf{q}, \omega)$

Most of our data were collected in the vicinity of the  $[1.5 \ 0 \ 0.2]$  position in reciprocal space, which, as far as  $q_{\parallel}$  is concerned, is the AF reciprocal point. In this geometry the magnetic inelastic intensity is proportional to  $S^{zz}(\mathbf{q}, \omega) + S^{yy}(\mathbf{q}, \omega) \approx 2S^{\perp}(q_{\parallel}, \omega)$ . In other words, only the fluctuations of spin components perpendicular to the chain direction contribute to the scattering.

Typical constant- $Q$  scans at  $Q = [1.5 \ 0 \ 0.2]$  (raw data) collected at several temperatures are shown in Fig. 2. A distinct peak is observed at  $(\hbar\omega) \approx 4 \text{ meV}$ . It is attributed to the low-lying excitation doublet from the Haldane ground state,

and is centered at the Haldane gap energy. The energy resolution in our experiments is not sufficient to resolve the splitting of the doublet by in-plane anisotropy.<sup>16</sup>

The magnetic cross section was measured by constant- $Q$  scans in the  $q_{\parallel}$  range  $0.47(2\pi)/a \leq q_{\parallel} \leq 0.53(2\pi)/a$ . The nonmagnetic background in the vicinity of the 1D AF point can be estimated by measuring the scattering at  $[1.4 \ 0 \ 0.2]$  and  $[1.6 \ 0 \ 0.2]$  for the same energy transfers. This approach is based on the fact that the dispersion along the chains is very steep, and the damping increases dramatically as  $q_{\parallel}$  deviates from  $\pi/a$ ; therefore at  $[1.6 \ 0 \ 0.2]$  the magnetic signal is absent, as shown in Fig. 2. At low temperatures the background correction was made using direct

point-by-point subtraction of the corresponding background scans from the signal. Although the background is roughly constant as a function of energy, there is some structure, most likely due to incoherent scattering from phonons. The magnetic scattering measured at elevated temperatures was analyzed under the assumption of a flat background.

To analyze our data we utilized the following empirical formula to describe the dispersion in the vicinity of the 1D AF planes:

$$\hbar\omega_{\perp}(q) = \sqrt{(\Delta_{\perp})^2 + c_0^2 \left( q_{\parallel} - \frac{\pi}{a} \right)^2}. \quad (1)$$

The cross section was taken in the double-Lorentzian form<sup>16</sup>

$$S^{\perp}(\mathbf{q}, \omega) = \frac{\hbar S_0^{\perp}}{\kappa_{\perp} \Gamma_{\perp}} \frac{1}{1 + [(q_{\parallel} - \pi/a)/\kappa_{\parallel}]^2 + \{\hbar[\omega - \omega_{\perp}(q_{\parallel})]/\Gamma_{\perp}\}^2}. \quad (2)$$

Here  $\Gamma_{\perp}$  is the fluctuation rate (intrinsic energy width), and  $\kappa_{\perp} = 1/\xi_{\perp}$  the inverse correlation length. The cross section (2), convoluted with the (1+3)-dimensional  $(E, \mathbf{Q})$  spectrometer resolution function, was fitted to the bulk of our data (simultaneously to all the constant- $Q$  scans) taken at  $T=7.8$  K, separately for samples A and B. The variable parameters were the prefactor  $S_0^{\perp}$ , and  $\Delta_{\perp}$ ,  $\kappa_{\perp}$ ,  $\Gamma_{\perp}$ , and  $c_0$ . The fitting results for both samples are summarized in Table I. Note that an excellent fit is achieved. The refined parameters are slightly different for samples A and B, which is possibly indicative of a difference in anisotropy constants. Some experimental data (background subtracted) are shown in Fig. 3 together with the data calculated using the refined parameter values. The simulated inelastic intensity as a function of  $q_{\parallel}$  and energy transfer ( $\hbar\omega$ ) is shown in a contour plot in Fig. 4. It can be seen that the shape of the intensity surface is strongly influenced by the experimental resolution, which is just barely sufficient for a quantitative measurement of  $S(\mathbf{q}, \omega)$ . The dispersion relation, calculated from the refined values for  $\Delta$  and  $c_0$ , is shown on the same plot.

The somewhat unconventional form, Eq. (2), for  $S(\mathbf{q}, \omega)$  was chosen, because it gives the theoretically predicted expression for the energy-integrated intensity  $S(\mathbf{q})$ . The latter has a square root Lorentzian (SQRL) form<sup>5,21,25</sup>

$$S(\mathbf{q}) \propto \frac{\xi}{\sqrt{1 + (q_{\parallel} - \pi/a)^2 \xi^2}}. \quad (3)$$

TABLE I. Refined parameters, characterizing the magnetic inelastic cross section  $S(\mathbf{q}, \omega)$  in NINAZ at  $T=7.8$  K.

	Sample A (protonated)	Sample B (deuterated)
$\Delta_{\perp}$ (meV)	3.53(3)	3.61(2)
$\kappa_{\perp}$ ( $\text{\AA}^{-1}$ )	0.054(22)	0.026(4)
$\Gamma_{\perp}$ (meV)	0.23(5)	0.13(3)
$c_0$ (meV $\text{\AA}$ )	168(6)	168(5)
$N_{\text{data}}^a$	280	380
$\chi^2$	0.99	1.03

<sup>a</sup>Number of data points used in fit.

We have also analyzed our data with a product-of-two-Lorentzians cross section. This procedure yields basically the same quality of fits and very similar refined parameter values. In other words, the quality of our data is not sufficient to

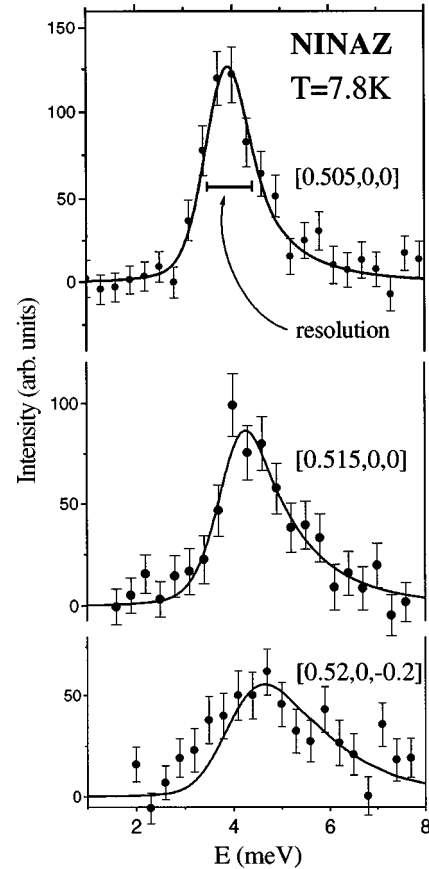


FIG. 3. Some typical constant- $Q$  scans collected on the deuterated sample B at  $T=7.8$  K. The background has been subtracted. The solid lines show the global fit with Eqs. (1) and (2). The horizontal bar shows the FWHM of the energy-projected resolution function ( $\approx 0.95$  meV at  $\hbar\omega = 4.5$  meV).

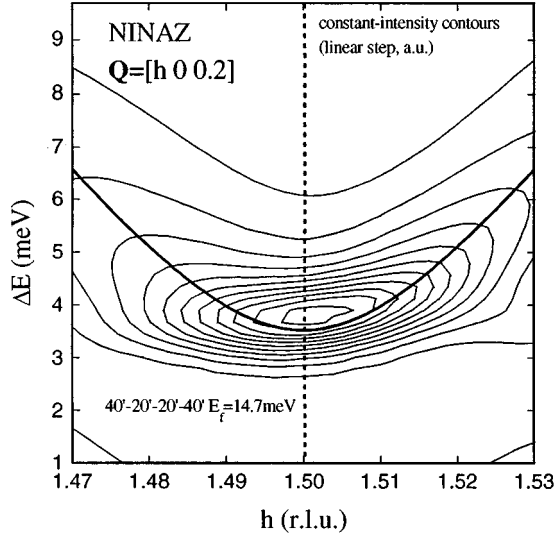


FIG. 4. Constant-intensity contours in  $[q_{\parallel}, (\hbar\omega)]$  space, simulated using Eqs. (1) and (2), the refined parameter values, and the known spectrometer resolution function. The heavy line shows the experimental dispersion relation (deuterated NINAZ,  $T=7.8$  K).

distinguish the two forms for the cross section.

After taking into account quantum renormalization corrections for the spin wave velocity in an  $S=1$  Heisenberg antiferromagnet,  $c_0$  may be used to obtain the value for  $J=c_0/(2.7a)\approx 10.73$  meV, which is reasonably consistent with the 12.5 meV value deduced from bulk measurements.<sup>17</sup> Note that the experimental ratio  $\Delta_{\perp}/|J|\approx 0.34$  for NINAZ is smaller than the theoretically predicted value of 0.41 for the isotropic case, and very similar to  $\Delta_{\perp}/|J|\approx 0.3$  observed in NENP,<sup>16</sup> even though the magnetic energy scale is different in the latter material. A relation between the gap energy  $\Delta_{\perp}$  and the exchange constant  $J$  for the *anisotropic* case was numerically obtained by Golinelli *et al.*,<sup>10-12</sup> and allows an estimate of the dimensionless ratio  $D/|J|\approx (0.41 - \Delta_{\perp}/|J|)/0.57\approx 0.17$  for NINAZ, which is also essentially equal to the value for NENP. The relation  $\Delta_{\zeta}\approx c_0$ , which is considered to be a fundamental characteristic of the Haldane phase, is satisfied by the refined parameter values, within the estimated standard deviations. The main constants, characterizing the Haldane systems NINAZ, NENP, and NINO, are compared in Table II.

### B. Temperature dependence

The inelastic scans at  $[1.5\ 0\ 0.2]$  were measured at several temperatures in the range 8–40 K for the deuterated sample

TABLE II. Experimental  $|J|$ ,  $\Delta$ , and  $D$  values in three quasi-1D  $S=1$  Haldane systems.

	NINAZ	NENP	NINO
$ J $ (meV)	10.7 <sup>a</sup>	4.7 <sup>b</sup>	4.5 <sup>c</sup>
$\Delta_{\perp}$ (meV)	3.61 <sup>a</sup>	1.23 <sup>b</sup>	1.2 <sup>d</sup>
$D$ (meV)	1.8 <sup>a</sup>	0.85 <sup>b</sup>	1.55 <sup>c</sup>

<sup>a</sup>This work.

<sup>b</sup>Renard *et al.* (Ref. 22); Regnault *et al.* (Ref. 16).

<sup>c</sup>Gadet *et al.* (Ref. 17).

<sup>d</sup>Hirota *et al.* (Ref. 23).

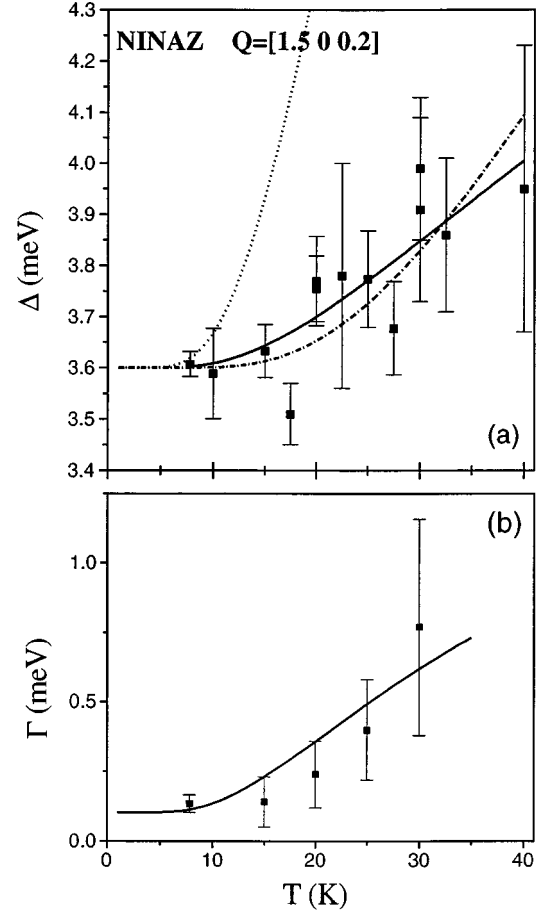


FIG. 5. (a) Measured temperature dependence of the Haldane gap  $\Delta_{\perp}$  in NINAZ. The solid line represents the best fit to the data using the empirical formula (5), with  $\Delta(0)=3.6$  meV and  $\alpha=0.4$  meV. The choice  $\alpha=2\pi\Delta(0)=22.6$  meV (dotted line) corresponds to Eq. (4), as predicted by field theoretical analysis (Refs. 26,27). The dot-dashed line is a fit to the empirical expression (7) with  $\delta=7.3$  meV. (b) Temperature dependence of the fluctuation rate (intrinsic energy width)  $\Gamma_{\perp}$  in Eq. (2). The solid line shows the best fit with Eq. (8) with  $\gamma=0.1$  meV and  $\Gamma_0=2.1$  meV.

(Fig. 2). The inelastic peak broadens progressively with increasing  $T$  and could not be observed above 50 K. The data were analyzed using Eqs. (1) and (2). The spin wave velocity  $c_0$  was assumed to be temperature independent and the 7.8 K value was used. Note that this assumption is required only to take proper account of the resolution effects and that the values for  $\Delta_{\perp}(T)$  extracted from the experimental  $E$  scans are practically independent of the actual value of  $c_0$ . Figure 5(a) shows the temperature dependence of the gap value  $\Delta_{\perp}$ .

There have been several theoretical works which predicted the temperature dependences of various characteristics of Haldane-gap systems, including that of  $\Delta$  (see, for example, Refs. 9,26,27). It is generally agreed that the Haldane gap shows activated behavior at  $T\rightarrow 0$ . From an analysis of the quantum nonlinear  $\sigma$  model Jolicoeur and Golinelli have derived the low- $T$  dependence of the Haldane gap in the isotropic (Heisenberg) case.<sup>27</sup>

$$\Delta(T)\approx\Delta(0)+\sqrt{2\pi\Delta(0)T}\exp\left(\frac{-\Delta(0)}{T}\right). \quad (4)$$

In the presence of easy-plane anisotropy the Haldane triplet is split, yielding two energy gaps  $\Delta_{\perp}$  and  $\Delta_{xx}$ . However, according to Sénéchal,<sup>26</sup> even relatively strong anisotropy does not change the  $T$  dependence appreciably. The low-temperature expression (4) should remain valid for the low-lying gap  $\Delta_{\perp}$ .<sup>27</sup> Equation (4), with  $\Delta_{\perp}(0)$  assumed to be 3.6 meV, is plotted as a dotted line in Fig. 5(a). Contrary to the theoretical expectations, it is clearly inconsistent with the experimental data on NINAZ.

Ma *et al.*<sup>28</sup> have used the form (4) to obtain the temperature dependence of the instantaneous spin correlation length  $1/\kappa(T) = c_0/\Delta(T)$  in NENP and compared the result to their experimental data. They too have found a strong discrepancy which they attributed to the fact that at high temperature; i.e., at  $T \gg \Delta$ , the nonlinear  $\sigma$  model is not applicable. For  $T < \Delta$  though, the nonlinear  $\sigma$  model was seen to agree reasonably well with the observed temperature dependence of the Haldane gaps in CsNiCl<sub>3</sub> and NENP.<sup>26,28</sup> It is important to emphasize that in our case of NINAZ the data were collected at  $T < \Delta_{\perp} \approx 40$  K, but the discrepancy is still very strong.

Having realized that Eq. (4) does not seem to work for NINAZ, we have analyzed our data using an empirically modified expression

$$\Delta(T) \approx \Delta(0) + \sqrt{\alpha T} \exp\left(\frac{-\Delta(0)}{T}\right). \quad (5)$$

The prefactor  $\alpha$  was treated as a parameter and refined to best fit the experimental points [again,  $\Delta(0)$  was fixed to 3.6 meV]. The refinement yields a good fit with  $\alpha = 0.38(0.13)$  meV [Fig. 5(a), solid line]. This is to be compared with the theoretical prediction  $\alpha = 2\pi\Delta(0) \approx 22.6$  meV for NINAZ.

Ma *et al.* have fitted their  $\kappa(T)$  data for NENP using another empirical formula<sup>28</sup>

$$\frac{1}{\kappa(T)} = \frac{1}{\kappa(0)} [1 - \exp(-\delta/T)], \quad (6)$$

where it is the activation energy  $\delta$  which is treated as an adjustable parameter. They found Eq. (6) to be consistent with their data in the entire experimental  $T$  range if  $\delta$  is taken somewhat larger (by a factor of approximately 1.4) than the lower Haldane gap  $\Delta_{\perp}$  in NENP. Note that this formula is radically different from Eqs. (4) and (5), since it is based on the idea that the energy scale relevant to the  $T$  dependence may be different from the Haldane gap value. Developing this approach, we have analyzed our  $\Delta_{\perp}(T)$  data for NINAZ with

$$\Delta_{\perp}(T) = \Delta_{\perp}(0) [1 - \exp(-\delta/T)]^{-1}, \quad (7)$$

which is equivalent to Eq. (6), assuming  $\Delta_{\perp} = c_0\kappa_{\perp}$ . Fixing  $\Delta_{\perp}(0) = 3.6$  meV and refining  $\delta$ , we obtain a very good fit [Fig. 5(a), dot-dashed line]. The refined value for the activation energy  $\delta = 7.3(0.4)$  meV is roughly twice as large as  $\Delta_{\perp}$ . In summary, the quality of our data does not allow us to distinguish between the two empirical forms (5) and (7), but Eq. (4) is definitely inapplicable to NINAZ.

Figure 5(b) shows the temperature dependence of the fluctuation rate  $\Gamma$  in Eq. (2). One expects an activated behavior<sup>16</sup>

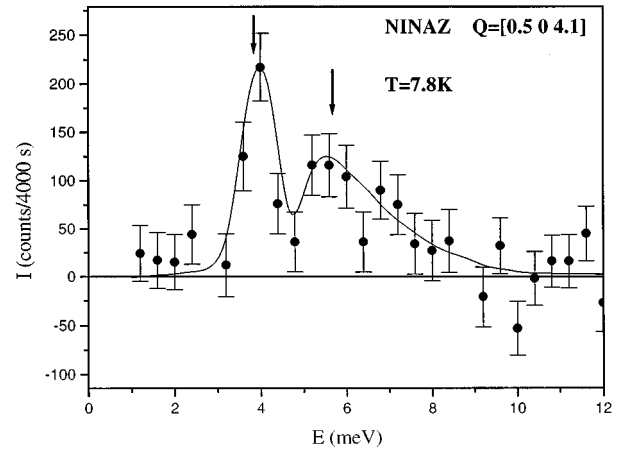


FIG. 6. Energy scan measured for the deuterated sample B at  $T = 7.8$  K and  $\mathbf{Q} = [0.5 \ 0 \ 4.1]$ , showing the two Haldane gap modes in NINAZ. The background has been subtracted. The solid lines is a guide to the eye.

$$\Gamma(T) \approx \gamma + \Gamma_0 \exp(-\Delta/T). \quad (8)$$

We have used the value 3.6 meV for the Haldane gap  $\Delta$ . Refining  $\Gamma_0$  and  $\gamma$  results in a reasonably good fit [Fig. 5(b), solid line] with  $\gamma = 0.1$  meV and  $\Gamma_0 = 2.1$  meV. Equation (8) appears to describe the experimentally observed dependence relatively well, but more precise measurements in a broader temperature range are required to clarify this point.

### C. Interchain interactions

To justify the approximation of replacing  $S(\mathbf{q}, \omega) = S(q_{\parallel}, q_{\perp}; \omega)$  by  $S(q_{\parallel}, \omega)$  we determined the gap value for different  $q_{\perp}$  at  $Q_{\parallel} = 1.5(2\pi)/a$ , that is, at the point where the longitudinal dispersion is a minimum. The measurements were performed on sample A at  $T = 7.8$  K. Within our experimental energy resolution [ $\approx 0.35$  meV half width at half maximum (HWHM)], no dispersion was observed. Therefore an upper limit can be set on the interchain exchange constant  $J'$ . Following the procedure used by Regnault *et al.*,<sup>16</sup> we obtain the limiting value  $J' \leq 0.008$  meV,  $|J'/J| \leq 7 \times 10^{-4}$ , which is at least as low as in NENP. This estimate is consistent with the fact that no long-range ordering<sup>17-19</sup> has been observed in NINAZ.

### D. Attempts to measure $S^{xx}(\mathbf{q}, \omega)$

An attempt was made to measure the gap value  $\Delta_{xx}$  for the out-of-plane spin component energy scans at  $\mathbf{Q} = [0.5 \ 0 \ 4.1]$ . The background was measured at  $\mathbf{Q} = [0.6 \ 0 \ 4.1]$  and  $\mathbf{Q} = [0.4 \ 0 \ 4.1]$ . In this geometry the inelastic intensity is roughly proportional to  $S^{xx}(q_{\parallel}, \omega) + S^{yy}(q_{\parallel}, \omega)$ . The magnetic signal is slightly weakened by the magnetic form factor of  $\text{Ni}^{2+}$ ,  $f_M \approx 0.9$ , for these  $Q$  values. Unexpectedly, the measurements were found to be heavily influenced by the mosaic spread of the crystal. The latter, after passing through the structural phase transition several times, was found to be as large as  $1.5^\circ$  for each domain type (see Fig. 1). The magnetic inelastic scattering is localized in thin ‘‘sheets’’ in reciprocal space [see Eq. (2)], i.e., at  $Q_{\parallel} \approx (2n+1)\pi/a$ . The crystal mosaic stretches the  $Q$ -space projection of the reso-

lution ellipsoid in the direction *perpendicular* to the scattering vector. Consequently there is a significant loss in intensity and  $q_{\parallel}$  resolution (defocusing), when the scattering vector is nearly parallel to the “sheets.” A further complication arises from the fact that the inelastic intensity at  $q_{\parallel} = \pi/a$  should scale<sup>16</sup> as  $1/\Delta$ . The numerical calculations of Golinelli *et al.*<sup>10</sup> suggest  $\Delta_{xx} \approx 0.41|J| + 1.41D \approx 6.5$  meV  $\gg \Delta_{\perp}$ . Therefore, the  $S^{xx}$  contribution to scattering is weakened. As a result, the  $\Delta_{xx}$  gap excitation is barely observable in the  $E$  scans at  $\mathbf{Q} = [0.4 \ 0 \ 4.1]$  (Fig. 6). No deconvolution analysis has been performed, due to the limited quality and quantity of data available. However, the experimentally determined value  $\Delta_{xx} \approx 6$  meV is in good agreement with the theoretical prediction.

#### IV. CONCLUSION

The quasi-1D Heisenberg antiferromagnet NINAZ was studied by single-crystal inelastic neutron scattering. The data were interpreted in the framework of the Haldane conjecture. The results indicate that NINAZ is in many ways

similar to the structurally related NENP and NINO, apart from the difference in the energy scale of magnetic interactions. The most intriguing result is the unusual temperature dependence of the Haldane gap which apparently is inconsistent with theoretical predictions.

#### ACKNOWLEDGMENTS

One of us (S.E.N.) would like to thank Brookhaven National Laboratory for hospitality and for facilitating extended visits. Work at the University of Florida was supported by the Division of Materials Sciences, U.S. Department of Energy, under Grant No. DE-FG05-92ER45280 (S.E.N.) and by the National Science Foundation through Grant No. DMR-9200671 (M.W.M.). Work at Brookhaven National Laboratory was supported by the Division of Material Sciences, U.S. Department of Energy, under Contract No. DE-AC02-76CH00016. Oak Ridge National Laboratory is managed by Lockheed Martin Energy Research Corp. for the U.S. Department of Energy under Contract No. DE-AC05-96OR22464.

\*Present address: Oak Ridge National Laboratory, P.O. Box 2008, Oak Ridge, TN 37831-6393.

- <sup>1</sup>F. D. M. Haldane, Phys. Lett. **93A**, 464 (1983).
- <sup>2</sup>F. D. M. Haldane, Phys. Rev. Lett. **50**, 1153 (1983).
- <sup>3</sup>I. Affleck, J. Phys. Condens. Matter. **1**, 3047 (1989).
- <sup>4</sup>G. Gomez-Santos, Phys. Rev. Lett. **63**, 790 (1989).
- <sup>5</sup>A. M. Tsvelik, Phys. Rev. B **42**, 10 499 (1990).
- <sup>6</sup>I. Affleck and R. A. Weston, Phys. Rev. B **45**, 4667 (1992).
- <sup>7</sup>R. Botet, R. Jullien, and M. Kolb, Phys. Rev. B **30**, 215 (1984).
- <sup>8</sup>I. Affleck, Phys. Rev. Lett. **62**, 474 (1989).
- <sup>9</sup>I. Affleck, Phys. Rev. Lett. **65**, 2477 (1990).
- <sup>10</sup>O. Golinelli, T. Jolicoeur, and R. Lacaze, Phys. Rev. B **45**, 9798 (1992).
- <sup>11</sup>O. Golinelli, T. Jolicoeur, and R. Lacaze, Phys. Rev. B **46**, 10 854 (1992).
- <sup>12</sup>O. Golinelli, T. Jolicoeur, and R. Lacaze, J. Phys. Condens. Matter **5**, 1399 (1993).
- <sup>13</sup>K. Nomura, Phys. Rev. B **40**, 2421 (1989).

- <sup>14</sup>M. P. Nightingale and H. W. J. Blote, Phys. Rev. B **33**, 659 (1986).
- <sup>15</sup>S. V. Meshkov, Phys. Rev. B **48**, 6167 (1993).
- <sup>16</sup>L. P. Regnault, I. Zaliznyak, J. P. Renard, and C. Vettier, Phys. Rev. B **50**, 9174 (1994).
- <sup>17</sup>V. Gadet, M. Verdaguer, J. P. Renard, J. Ribas, C. Diaz, M. Montfort, X. Solans, C. P. Landee, J. P. Jamet, and A. Dworkin (unpublished).
- <sup>18</sup>J. P. Renard *et al.*, J. Magn. Magn. Mater. **90**, 213 (1990).
- <sup>19</sup>L. K. Chou *et al.*, Physica B **194-196**, 313 (1994).
- <sup>20</sup>J. P. Renard *et al.*, Europhys. Lett. **3**, 945 (1987).
- <sup>21</sup>S. Ma *et al.*, Phys. Rev. Lett. **69**, 3571 (1992).
- <sup>22</sup>J. P. Renard *et al.*, J. Appl. Phys. **63**, 3538 (1988).
- <sup>23</sup>K. Hirota, S. M. Shapiro, K. Katsumata, and M. Hagiwara, Physica B **213**, 173 (1995).
- <sup>24</sup>L. K. Chou, Ph.D. thesis, University of Florida, 1995.
- <sup>25</sup>H. Mutka *et al.*, Phys. Rev. Lett. **67**, 497 (1991).
- <sup>26</sup>D. Sénéchal, Phys. Rev. B **47**, 8353 (1993).
- <sup>27</sup>T. Jolicoeur and O. Golinelli, Phys. Rev. B **50**, 9265 (1994).
- <sup>28</sup>S. Ma *et al.*, Phys. Rev. B **51**, 3289 (1995).